Chapter

Vital Sign Measurement Using FBG Sensor for New Wearable Sensor Development

Shouhei Koyama and Hiroaki Ishizawa

Abstract

In this study, we measured the vital signs of a living body using an FBG sensor by installing it at a pulsation point such as the radial artery. We developed a biological model to demonstrate the capability of an FBG sensor. The FBG sensor signal was found to correspond to the changes in diameter of the artery caused by the pressure of the blood flow. Vital signs such as pulse rate, respiratory rate, stress load, and blood pressure were calculated from the FBG sensor signal. While pulse rate and respiration rate were calculated by peak detection of FBG sensor signal. Blood pressure was calculated from the waveform shape of one beat of the FBG sensor signal by PLS regression analysis. All vital signs were calculated with high accuracy. The study helps establish that these vital signs can be calculated continuously and simultaneously. Considering that an FBG sensor can detect a strain with high sensitivity using a small optical fiber, it is expected to be adopted widely as a novel wearable vital sign sensor.

Keywords: FBG sensor, pulse rate, respiration rate, blood pressure, wearable sensor

1. Introduction

In Japan, there is surge in demand for medical care of the elderly as their population continues to increase [1]. This is causing a serious concern especially considering the prevailing shortage of medical staff. Meanwhile, since the Tokyo Olympic Games will be held in 2020, there is a high need for self-healthcare management among healthy people. A simple home health system to monitor the vital signs in elderly people is becoming an absolute necessity, as there is increasing demand for their self-health management on a daily basis. Vital signs are fundamental indicators of human health. These indicators include heart rate, respiration rate, blood pressure, body temperature, level of consciousness.

In order to meet such needs, wearable sensors are being developed by manufacturers to monitor vital signs [2–4]. These sensors are glasses or wristwatch type, they have a characteristic that can measure vital signs continuously. Most of these sensors are of photoelectric pulse wave type measuring the changes in light absorption caused by hemoglobin in blood vessels. These sensors are compact, portable, and easy to install on a human body. However, there are a few issues with these sensors: moisture noise caused by perspiration, skin damage due to the probe pressure [5], and dependence of signal strength on probe mounting position [6]. In addition, people have psychologically stressful for people who do not use wrist watches or

eyeglasses from attaching these type wearable sensor. Many photoelectric pulse wave sensors can measure only the pulse rate and cannot measure blood pressure. The currently used measuring many sphygmomanometers are of stationary type and therefore cannot be carried by hand. Accordingly, they are not suitable for home use and continuous monitoring.

The FBG sensor is an optical fiber type highly accurate strain sensor. The FBG sensor has a feature that a plurality of sensors can be installed with one interrogator, the optical fiber length is 1 km or more. From these features, FBG sensors are used in building and civil engineering fields. Tam et al. have introduced FBG sensors in railway rail monitoring systems [7, 8]. There are research studies reporting measurement of vital signs using FBG sensors [9–11]. Furthermore, since the sensor part is an optical fiber, it can be introduced into a textile product [12]. Therefore, the FBG sensor is introduced into the wristband or the sleeve of the shirt, and the sensor can be installed on the living body simply by wearing the textile product.

The authors propose that the FBG sensor is installed to the pulsation point of the skin surface and the vital sign can be calculated from the measured signal. The vital signs such as pulse rate, respiratory rate, stress load, and blood pressure are calculated from the measured signal of FBG sensor. In this paper, the details of the strain signal measured at a pulsation point of a human body with the FBG sensor, method of calculation from the measured signal, and measurement accuracy for each vital sign are described.

2. FBG sensor system

An FBG sensor system is composed of an interrogator part with a light source and a detector, and a sensor part with an optical fiber. The schematic and the specifications of the FBG sensor system used in this study are shown in **Figure 1** and **Table 1**, respectively. We used the FPG interrogator system, named PF25-S01 (Nagano Keiki Co., Ltd.) [13]. This interrogator is equipped with an ASE light source that emits near infrared light with a wavelength of 1525–1570 nm that passes through the core of the optical fiber.

In the FBG sensor, a diffraction grating is formed when the refractive index is periodically changed along the axis of the core of the optical fiber. The FBG sensor reflects only a specific wavelength corresponding to the interval period of the diffraction grating. The wavelength of the reflected light from the FBG is called Bragg wavelength that follows the Eq. (1),

$$\lambda_{Bragg} = 2n_{eff}\Lambda \tag{1}$$

where, λ_{Bragg} is the Bragg wavelength, n_{eff} is the effective refractive index of the grating portion, and Λ is the grating interval. Since the effective refractive index is constant during a measurement, the Bragg wavelength changes accordingly as the lattice spacing changes. Therefore, when the Bragg wavelength varies, the lattice spacing changes due to the strain in the sensor part. Any distortion applied to the sensor section is detected based on this principle.

The Bragg wavelength reflected by the sensor portion passes through a circulator and is directed to a detection device that is a Mach-Zehnder interferometer. The optical path difference of the interferometer is approximately 5 mm. The homodyne detection method using the Mach-Zehnder interferometer detects the shift length of Bragg wavelength as interference phase shift [14, 15]. The Mach-Zehnder interferometer provides the light outputs through three detectors.

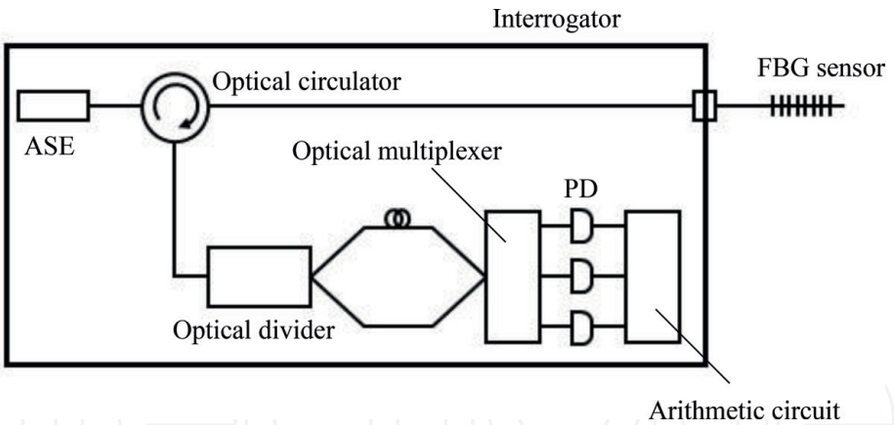

Figure 1.
FBG sensor system.

Interrogator		**Optical fiber**	
Size D × W × H (mm)	230 × 330 × 100	Material	Silica glass (Core: Ge)
Weight (kg)	4	Mode	Single mode
Light source	ASE	Fiber diameter (μm)	250
Wavelength (nm)	1525–1570	Cladding diameter (μm)	145
Power (mW)	30	Core diameter (μm)	10.5
Sampling rate (kHz)	10	Detection range (nm)	1550 ± 0.5
Detector	InGaAs PIN PD		
Wavelength resolution (pm)	±0.1		

Table 1.
Specification of FBG sensor system.

In each detector, the detected light is photo-electrically converted into an electric signal that is further converted to a digital signal by an analog/digital converter. Subsequently, the phase angle is demodulated, and a wavelength shift (proportional to the displacement and distortion) is calculated. The method has an advantage in that the resolution of wavelength measurement is finer compared with other methods. By this method, the pressure of the FBG sensor part is detected by measuring the displacement in Bragg wavelength.

3. Relationship between human body signal and FBG sensor signal

Experiments were performed using a biological model (**Figure 2**) to study the signals measured by an FBG sensor attached to a living body. A piston was employed to simulate the heart, and a blood-mimicking fluid (manufactured by CIRS) was used to simulate the blood. The movement of the piston was controlled to set the flow rate of the pseudo blood passing through a 500-mm-long acrylic pipe (inner diameter 8 mm) that simulated a blood vessel. For a phantom biological model, Flow Phantom (Supertech, Inc., ATS 524), was used. A flow phantom, made of a rubber material, was used to simulate the resilience of a living body (artificial skin), and it was provided with a hole of 8 mm diameter located at a depth of 15 mm from the top surface. A pipe of 8 mm inner diameter, made of vinyl

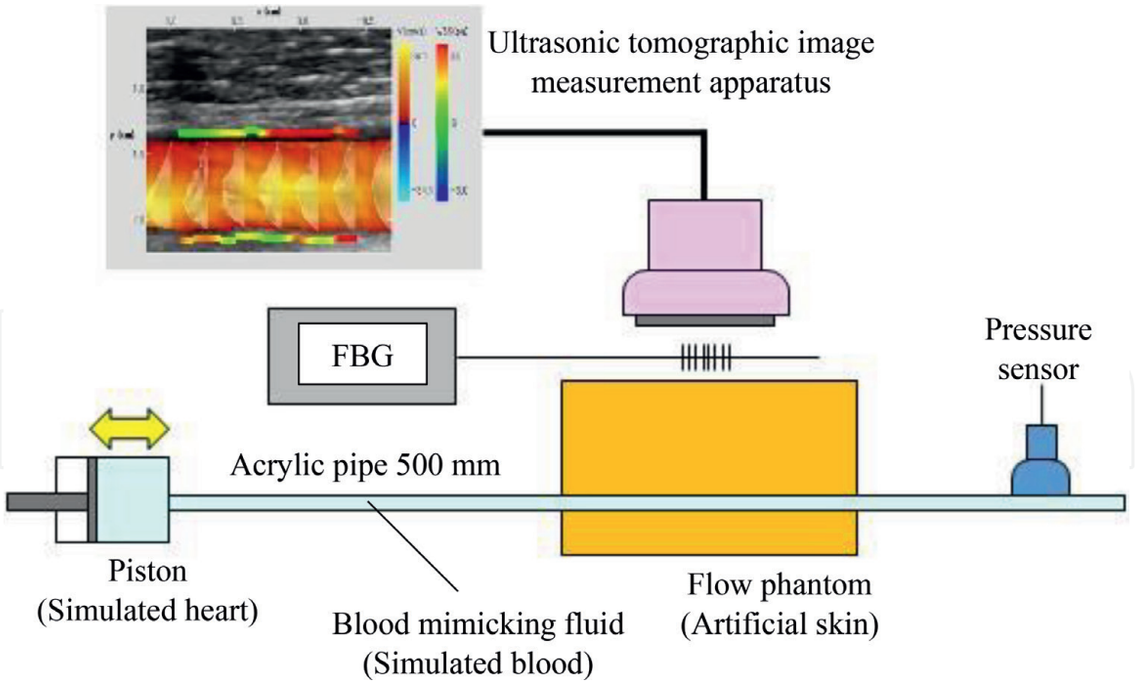

Figure 2.
Schematic of a biological mode.

chloride, and a sensor to measure the pressure of the pseudo blood were installed at the rear of the flow phantom. The pseudo blood, discharged from the piston, passed through the acrylic pipe, flow phantom, and vinyl chloride pipe in this order. An FBG sensor was attached on top of the flow phantom perpendicular to the direction of flow of the pseudo blood. The sensor part of an ultrasonic tomographic image measurement apparatus, installed parallel to the direction of flow of the pseudo blood and covering the FBG sensor as shown in **Figure 2**, captures the image of the inner details of the flow phantom [16].

During the flow of the pseudo blood, the changes in the inner diameter of the pseudo artery were measured by the FBG sensor and the tomographic apparatus. The FBG sensor signal for a flow rate of 30 mL of pseudo blood in 0.5 s, the diameter of the simulated artery from the tomographic image, and the result of the pressure gauge are shown in **Figure 3**. It is evident that the FBG sensor signal is closely similar to the diameter of the simulated artery and the pressure of the fluid. In addition, **Figure 4** shows the FBG sensor signal for various conditions of the pressure of

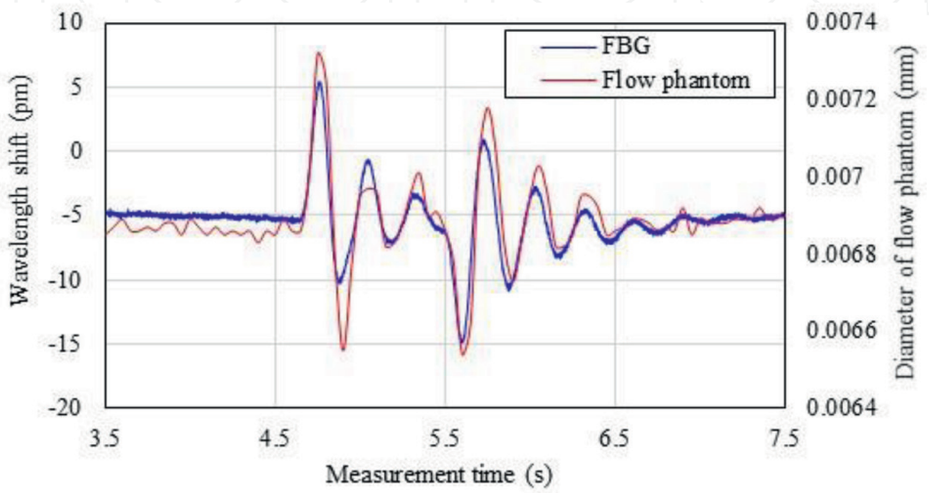

Figure 3.
Result of flow phantom diameter and FBG sensor signal.

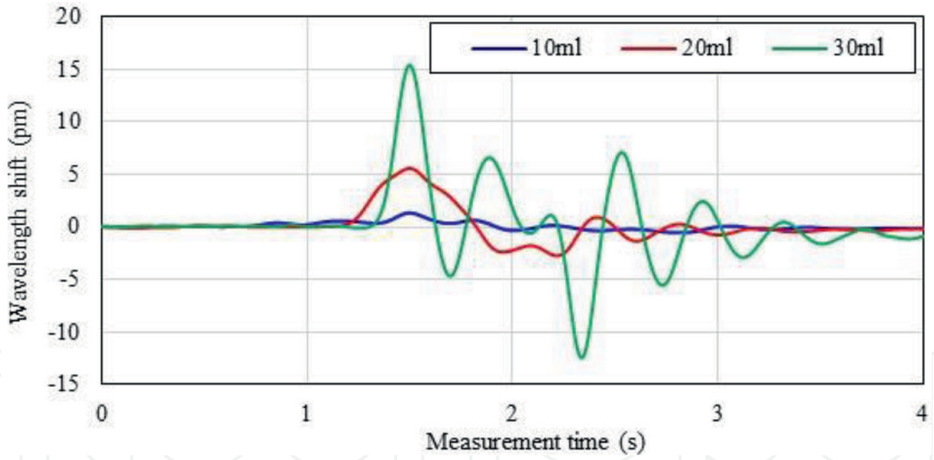

Figure 4.
Result of FBG sensor signal while changing the pressure.

the pseudo blood. It is evident that the larger the pressure of the simulated blood is, the larger the amplitude of the FBG sensor becomes. In this way, it was confirmed that the FBG sensor signal could measure the variations in the artery diameter caused by the blood pressure. In other words, as the strain at the pulsation point is changed by the pressure of the blood flow, the magnitude of the strain change is measured by the FBG sensor; this observation indicates that the FBG sensor signal contains information on blood pressure.

4. Relationship of heartbeat and FBG sensor signal

In Section 3, it was found that the variation in diameter of the blood vessel could be measured by the FBG sensor. In this section, we discuss the relation between the FBG sensor signal and heartbeat by installing the FBG sensor at a pulsation point of the subject.

The FBG sensor was installed perpendicular to the direction of blood flow in the radial artery at the wrist of the subject. An electrocardiograph (Nihon Kohden Corp., PVM-2701) was installed at the chest of the subject, and the electrocardiogram was measured simultaneously. The subject was male in their twenties, their posture at the time of measurement was supine, the sampling rate was 10 kHz, and the duration of measurement was 30 s. The peak-to-peak interval (PPI) of the FBG sensor signal and the R-to-R interval (RRI) of the electrocardiogram were calculated.

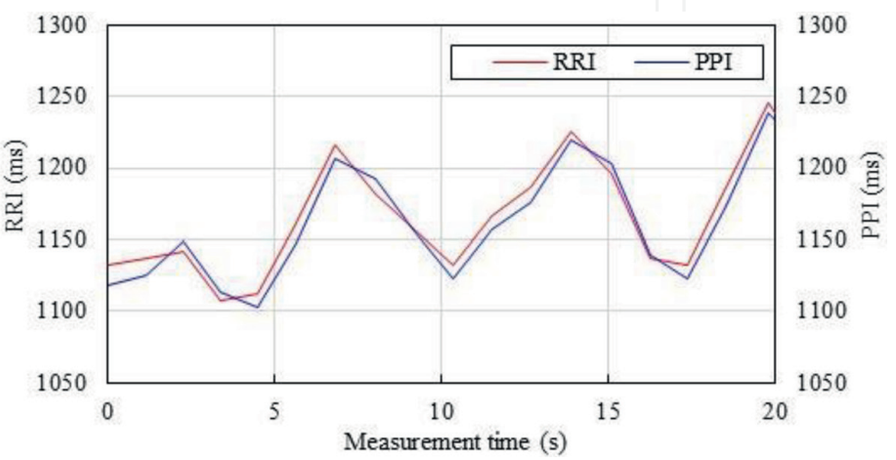

Figure 5.
Results of RRI and PPI.

The result of the RRI and PPI of the subject is shown in **Figure 5**, where the horizontal axis is the measurement time, and the vertical axes are the time intervals of PPI and RRI [17]. The heart rates of subject was ~51 times per min. It is evident that the RRI and PPI plots are almost identical for the subject. In other words, the FBG sensor signal corresponds to the heartbeat vibration as it represents the variation in the diameter of the arterial blood vessel caused by the flow rate (or pressure) that in turn is related to the heartbeat.

5. Vital sign calculation from peak in FBG sensor signal

5.1 Calculation of pulse rate

Since the FBG sensor corresponds to heartbeat vibration, the vital sign can be calculated from the FBG sensor signal. In this section, the pulse rate is calculated from the FBG sensor signal. An FBG sensor was installed perpendicular to the direction of blood flow in the radial artery at the left wrist of the subject. In order to measure the reference pulse rate, an electronic sphygmomanometer was installed at the upper arm of the subject. The measurements using the FBG sensor and the electronic blood pressure were performed at the same time. The peak interval (PPI) of the FBG sensor signal was measured, and the pulse rate per min was calculated from Eq. (2).

$$PR_{cal}(times/minutes) = PPI/60 \tag{2}$$

where, PR_{cal} is calculated pulse rate, and PPI is the peak interval. Three subjects were measured in supine position, and the measurement conditions were the same as those for the experiment on heartbeat discussed in Section 4.

A scatter diagram between the reference pulse rate and the pulse rate calculated from the FBG sensor signal is shown in **Figure 6**. The correlation coefficients for

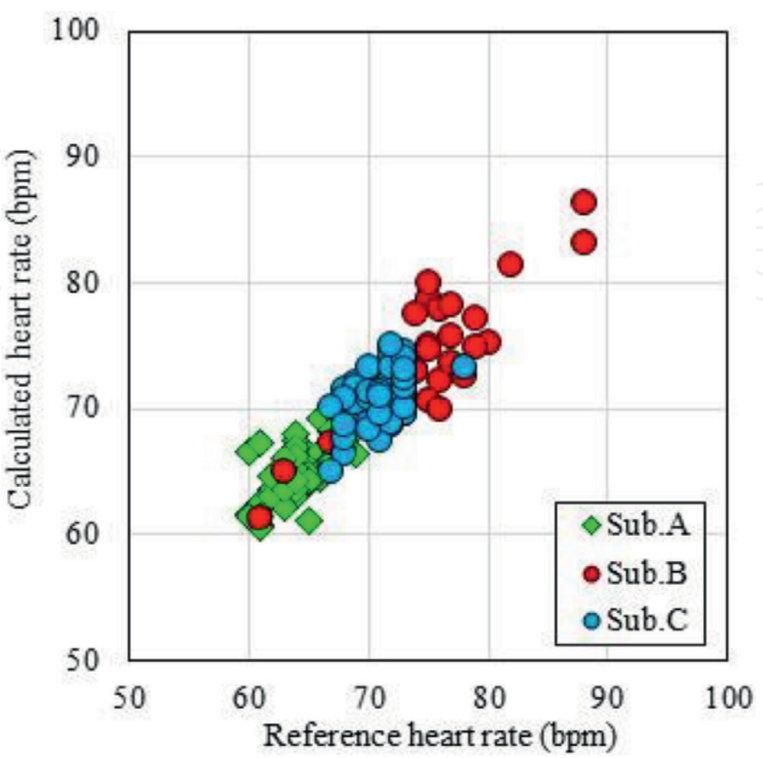

Figure 6.
Result of calculated pulse rate from FBG sensor signal.

the subjects A, B, and C were observed to be 0.67, 0.87, and 0.56, respectively, while the respective measurement accuracies were 2.1, 2.6, and 1.9 bpm. These results indicate that the pulse rate could be measured from the FBG sensor signal with high accuracy. Thus, it is evident that the pulse rate can be calculated if the peak of the FBG sensor signal is detected accurately.

5.2 Calculation of respiratory rate

The pulse rate was calculated from the FBG sensor signal in Section 5.1. This section describes the measurement and calculation of respiration rate. When a person breathes, a physiological phenomenon called respiratory dynamic arrhythmia occurs, whereby the pulse rate rises during inspiration and decreases during expiration. In other words, the PPI decreases during inspiration, and increases during expiration. Therefore, when breathing is repeated, the PPI cycles up and down, and thus, the period of a breath cycle can be deduced from a PPI cycle. The respiratory rate per min is calculated from Eq. (3),

$$RR_{cal} = PPI_{cyc}/60 \tag{3}$$

where, RR_{cal} is calculated respiration rate, and PPI_{cyc} is the cycle of PPI.

Experiments on breathing rate were conducted with three subjects. To measure the reference respiratory rate, a medical face mask attached with a temperature data logger (Ishikura Shoten Co., Ltd., SK-L200 THII) was used. The purpose of the face mask was to prevent the breath from leaking out. Breath temperature is known to be higher than the atmospheric temperature. At the time of inspiration, the temperature of the atmosphere is measured with a data logger. On the contrary, as the breath temperature was measured at exhalation, the value was relatively higher. Thus, a constant periodic temperature change was measured every time the subject breathes. One cycle of this temperature change was used as reference respiration time, and the reference respiratory rate was calculated from Eq. (3). The FBG sensor signal was measured under the same conditions as those for the experiment on pulse rate presented in Section 5.1. The subjects were in sitting posture at the time of measurement.

The results of the temperature data logger and PPI from the FBG sensor signal are shown in **Figure 7**. It is evident that both curves are very similar to each other. In addition, it could be confirmed that the cycle varies depending on the number of breaths. The respiratory rates calculated from the temperature data logger and the FBG sensor signal are plotted against one another in **Figure 8** for the three

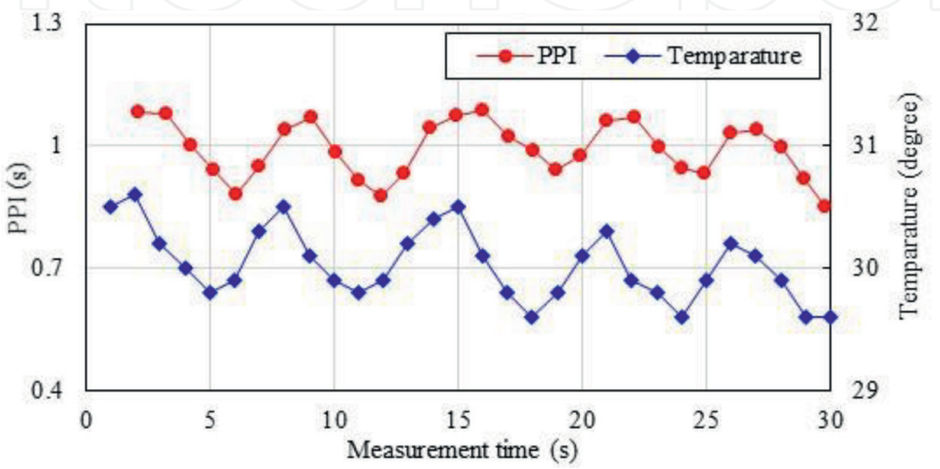

Figure 7.
Results of the PPI from the temperature data logger and the FBG sensor.

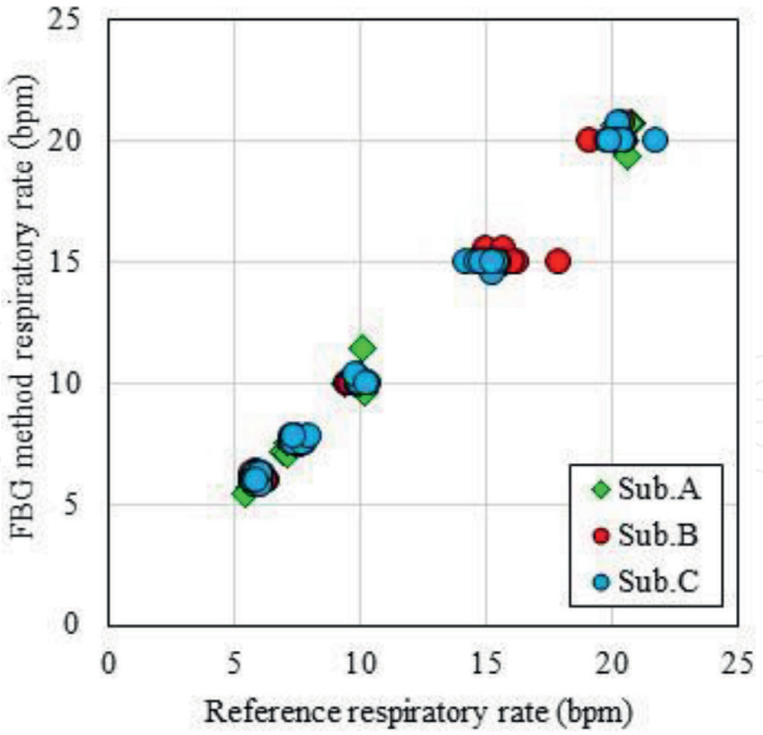

Figure 8.
Result of calculating respiratory rate.

subjects. The measurement accuracies observed for the three subjects were 0.4, 0.6, and 0.4 per min, which were considered to be reasonably good. The high measurement accuracy was observed even for different respiration rates of the same subject and for different subjects. The change in pulse rate (change in PPI interval) due to respiratory dynamic arrhythmia was very small; however, since the sampling rate of the FBG sensor was 10 kHz, it is considered that the calculated respiratory rate was accurate. This measurement method can calculate a respiratory rate in the range of 6–10 bpm; therefore, it is suitable for measurement of slow breathing (~12 bpm or less). It is evident from the above results that the high accuracy of measurement of respiratory rate is attributable to the high sampling rate.

6. Calculating of blood pressure from the waveform of FBG sensor signal

6.1 Waveform of the FBG sensor signal

In this section, the blood pressure is calculated from the waveform of the FBG sensor signal. As shown in Section 3, the FBG sensor signal is measured representing the pressure of the blood flow that causes a change in the diameter of the blood vessel. Pulsation is a distortion that causes an arterial distortion on the skin surface. Therefore, information on blood pressure is considered to be present in the FBG sensor signal from which a distortion is measured.

A signal measured with a general photoelectric pulse wave sensor is a volume pulse wave signal indicating the volume of blood. A signal obtained by second derivative of the volume pulse wave signal is an acceleration plethysmogram. The basic shape of acceleration plethysmogram includes five peaks [18]. The A-wave to the E-wave are called initial systolic positive wave, initial contraction negative wave, mid-systole re-elevation wave, post-contraction descent wave, and expansion initial positive wave, respectively. Therefore, an acceleration pulse wave contains information on systole and diastole of the heart. The first derivative signal of the

FBG sensor is similar to the acceleration pulse wave in shape [13]. Since an FBG sensor signal indicates the displacement of the Bragg wavelength due to strain, time change of the volume pulse wave is measured. Therefore, the first derivative signal of the FBG sensor is similar to the second derivative signal of the volume pulse wave signal. Furthermore, since the first derivative waveform of an FBG sensor signal includes information on the systole and diastole of the heart, the blood pressure can be calculated from this waveform.

6.2 Calculation method of blood pressure from the FBG sensor signal

When blood pressure was calculated from FBG sensor signal, PLS regression analysis, which is a widely known multivariate analysis among others, was used. The PLS regression analysis can construct calibration curves from the explanatory and objective variables. At this time, it is a feature to construct a calibration curve on the premise that an explanatory variable and an objective variable contain errors. The explanatory variable is the FBG sensor signal waveform, and the objective variable is the blood pressure measured simultaneously by the electronic sphygmomanometer. The FBG sensor signal is processed through the following steps [19].

1. The FBG sensor signal is processed with a band pass filter of 0.5–5 Hz.

2. The 'A' peak ('A' wave) is detected from the signal waveform of the band pass filter.

3. The signal is divided for each detected peak.

4. The divided signals are averaged.

5. At the vertical axis of the averaged signal, the first point (peak of 'A' wave) is normalized to "1", and the lowest point (peak of 'B' wave) is set to "0".

6. The horizontal axis of all FBG sensor signal waveforms processed up to the 5th term is cut out in the shortest time, and the length of the horizontal axis is unified.

The step 1 of the signal processing a range for covering a signal with a pulse rate of 30–300 times/min. In step 4 of the signal processing, considering that the measurement time of the electronic sphygmomanometer is ~30 s, the average is calculated for the pulse wave signals measured within that time. The step 5 of signal processing is to cancel the vertical axis fluctuations caused by pressure while installing the FBG sensor in humans. The step 6 of signal processing is to cancel the pulse rate fluctuations caused by respiratory sinus arrhythmia.

The FBG sensor signal processed through the aforementioned signal processing steps is used as an explanatory variable, the blood pressure value of the electronic sphygmomanometer measured simultaneously is used as a target variable, and a calibration curve is constructed by PLS regression analysis. The newly measured FBG sensor signal is substituted into this calibration curve to calculate the blood pressure.

6.3 Experimental result of calculating the blood pressure

This experiment was performed on three subjects. A schematic of the experimental blood pressure measurement is shown in **Figure 9** [19]. The posture of the subject was supine, and the FBG sensor was installed at the pulsation point of the radial artery of the right wrist. The reference blood pressure value (objective

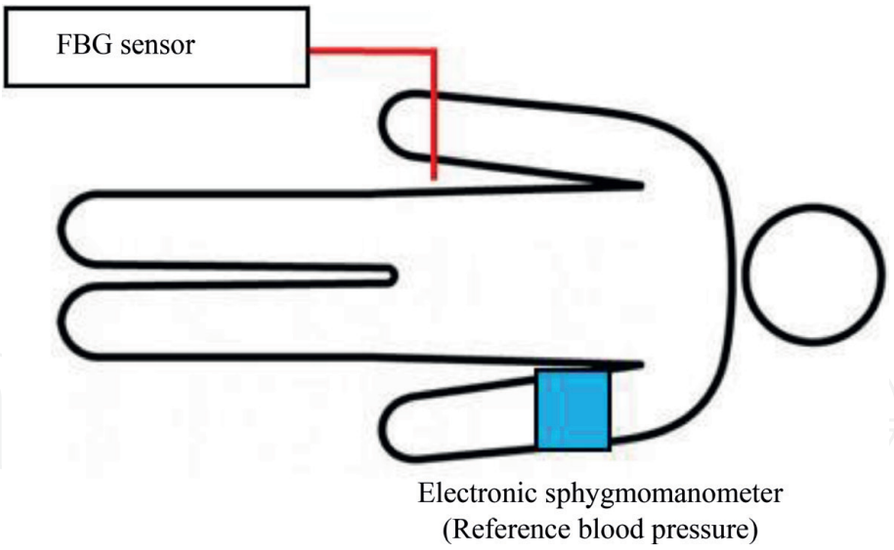

Figure 9.
Experimental image of blood pressure measurement.

variable) was measured simultaneously with the electronic sphygmomanometer installed at the left upper arm. Systolic and diastolic blood pressures were measured with an electronic sphygmomanometer. In the calculation of the systolic blood pressure, the signal-processed FBG sensor signal waveform was used as an explanatory variable, and the systolic blood pressure measured simultaneously with the electronic blood pressure monitor was used as the objective variable. Similarly, in the calculation of the diastolic blood pressure, the same FBG sensor signal waveform and the diastolic blood pressure measured simultaneously with electronic sphygmomanometer were used. The measurement time was 30 s, while the number of measurements was 75 times. Whereas 50 data points were used for construction of calibration curve, the remaining 25 data points were assigned to the calibration curve and used as verification data for blood pressure calculation. The target measurement accuracy was ±5 mmHg.

Table 2 shows the calibration curve construction data sets of systolic and diastolic blood pressures in each subject [19]. A calibration curve for calculating systolic blood pressure or diastolic blood pressure was constructed using the data sets of each subject. **Table 3** shows verification data sets for calculation of systolic and diastolic blood pressures for each subject. The verification data set is substituted into the constructed calibration curve, and systolic and diastolic blood

Subject	Number	Max (mmHg)	Min (mmHg)	Ave (mmHg)
(a) Systolic blood pressure data set				
A	50	125	100	111.3
B	50	136	113	123.1
C	50	111	93	100.9
(b) Diastolic blood pressure data set				
A	50	79	46	62.7
B	50	80	56	68.2
C	50	60	46	53.7

Table 2.
Calibration curve construction data sets.

Subject	Number	Max (mmHg)	Min (mmHg)	Ave (mmHg)
(a) Systolic blood pressure data set				
A	25	131	100	110.1
B	25	138	112	122.2
C	25	110	93	100.4
Average systolic blood pressure in data set (mmHg)				110.9
(b) Diastolic blood pressure data set				
A	25	77	46	60.3
B	25	76	58	68.0
C	25	65	39	53.1
Average diastolic blood pressure in data set (mmHg)				60.5

Table 3.
Verification data set in each subjects.

pressures were calculated. For example, a calibration curve was constructed with 50 data points of the systolic blood pressure of the subject A; the 25 data points of the systolic blood pressure of verification data of the subject A were substituted into the calibration curve, and the systolic blood pressure of subject A was calculated. Similarly, a calibration curve was constructed with 50 data points of the diastolic blood pressure of the subject B in **Table 2**; the 25 data points of validation data of the diastolic blood pressure of the subject B in **Table 3** were substituted into the calibration curve, and the diastolic blood pressure of subject B was calculated.

Figure 10 shows a scatter plot of reference blood pressure and calculated blood pressure during systole and diastole of each subject. **Table 4** shows the results of blood pressure calculation, whereby it was observed that the calculation accuracy of systolic and diastolic blood pressures were ±5 mmHg, and it was calculated with the same blood pressure value as that of a commercially available blood pressure monitor. In the case of the systolic blood pressure, the average value of the verification data for blood pressure calculation was 110.9 mmHg, while the average value

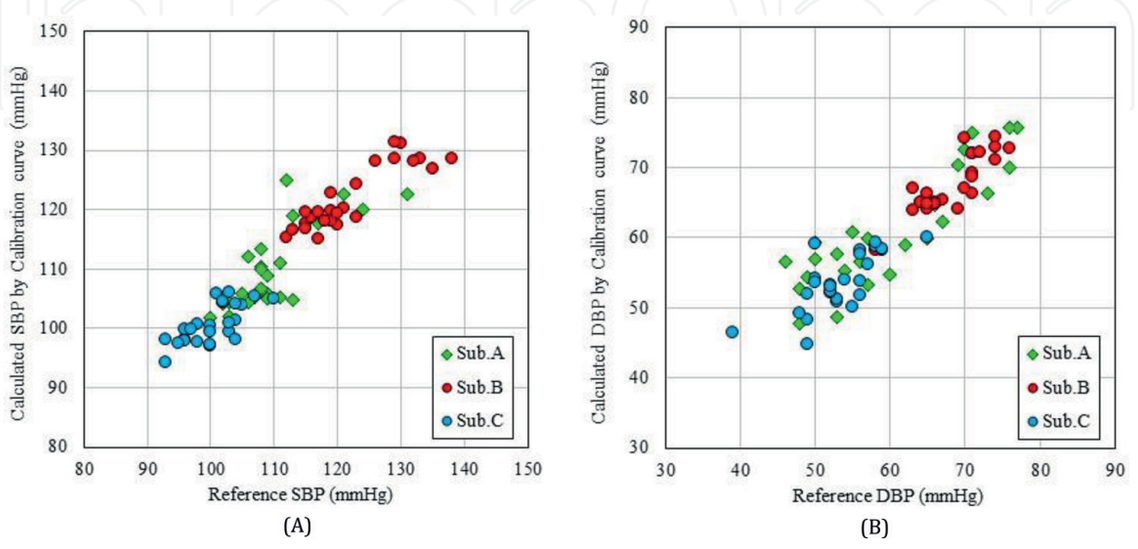

Figure 10.
Scatter plot of reference blood pressure and calculated blood pressure during systolic and diastolic. (A) Calculated result in systolic blood pressure. (B) Calculated result in diastolic blood pressure.

	Subject	A	B	C	Average
Calculating accuracy (mmHg)	Systolic	3.4	2.8	2.6	2.9
	Diastolic	4.1	1.8	2.6	2.8

Table 4.
Results of calculating blood pressure.

of the calculation accuracy was 2.9 mmHg (~2.6%). Similarly, in the diastolic blood pressure, the average value of the verification data for blood pressure calculation was 60.5 mmHg, while the average value of the calculation accuracy was 2.8 mmHg (~4.7%). These results indicate that the calculation accuracy of diastolic blood pressure is lower than that of systolic blood pressure. This is due to step 6 of signal processing, whereby the canceling of the pulse rate fluctuation was performed in order to calculate the FBG sensor signal by the PLS regression analysis. The so-called latter half portion of a single beat of the FBG sensor signal is truncated. There is a peak of expansion initial positive wave in this part, which represents the diastole of the heart. Therefore, it is considered that the deletion of the diastolic information from the FBG sensor signal caused a decline in the calculation accuracy. In other words, in this calculation method, since the negative characteristics of the signal processing is reflected in the result, the blood pressure is calculated from the movement of the heart included in the FBG sensor signal. However, considering that the results of all blood pressure calculations were ±5 mmHg, it is considered that the blood pressure was calculated with high calculation accuracy. Therefore, it is established that the blood pressure can be calculated with high calculation accuracy by constructing the calibration curve by PLS regression analysis of the waveform of the FBG sensor signal. It is evident from this result that it is possible to calculate blood pressure from the same FBG sensor signal in addition to pulse rate, respiratory rate, and stress load.

7. Conclusion

In this paper, the method of calculating each vital sign from the FBG sensor signal was described. An experiment using a biological model demonstrated that the FBG sensor signal was influenced by the change in diameter of the tube through which a fluid (pseudo blood) was allowed to flow by a simulated pressure. This model was replaced with a living body, and a change in the diameter of the artery caused by a change in the flow rate of blood related to the movement of the heart was measured. The FBG sensor signal was measured at a high temporal resolution of 10 kHz; therefore, the pulse rate could be calculated with a high measurement accuracy. Based on the phenomenon of respiratory sinus arrhythmia, the respiration rate could be calculated from the cycle of pulse rate change during expiration and inspiration. On the other hand, the first derivative waveform of the FBG sensor signal was found to be similar to the acceleration pulse wave, which was the second derivative of the volume pulse wave signal; therefore, it was considered that the systolic and diastolic information of the heart was present in the signal. Subsequent to the signal processing of this primary derivative waveform of FBG sensor signal, a calibration curve was constructed by PLS regression analysis for calculating the blood pressure, and accordingly, the blood pressures (systolic and diastolic) were calculated with high accuracy. All these vital signs were calculated from a measured FBG sensor signal. Therefore, considering that only the analysis method is different, it is possible to calculate a plurality of vital signs simultaneously from one measurement signal. Since the FBG sensor signal is continuously measured, the vital signs

can also be calculated on a continuous basis. In addition, the signal is measured simply by installing the FBG sensor at the pulsation point. Apart from the wrist, there are other pulsation points such as at the elbow, neck, temple, and ankle of the living body. Therefore, it is possible to select a part of interest that can be easily measured. Since the FBG sensor is an optical fiber, it can be introduced into a textile product. Cover the optical fiber with multiple silk thread in technic of braid. Unevenness is formed on the surface of the optical fiber by this silk thread, and frictional force is occurred. The optical fiber covered with this silk thread is embedded into the knitted fabric by inlay knitting. With this method, the optical fiber can be fixed without slipping in the knitted fabric. If FBG sensor can be introduced into textile products, it can be applied to wristbands, long-sleeved shirts, socks, and various other products. However, there are issues such as miniaturization of the FBG interrogator.

There are two approaches to applying the FBG sensor system in the clinical setting. First method, place the current FBG interrogator in the corner of the room, extend the optical fiber and install the FBG sensor in the hospitalized patient. With this method power supply can be supplied stably. The second method is to develop a compact FBG interrogator that can be attached to the human body. We are developing the 1/12 downsizing prototype FBG interrogators (74 × 97 × 57 mm, 175 g) using commercially available optical components. This interrogator is battery-powered and wirelessly communicates measurement signals. If electronic circuits etc. are changed from commercial type to specialization type, further size down is predicted. This prototype FBG interrogator can be operated at minimum 5 hours with battery. However, it is necessary to take measures against the temperature caused by heat. In our study, we employed the FBG sensor commonly used in applications ranging from infrastructure to living organisms. While we used only one FBG sensor for all our experiments, the length of the optical fiber was also very short. The currently available commercial FBG interrogators have been specifically developed for use in large-scale applications employing many sensors. Our research is a highly original theme that is entirely different from the current application areas of FBG sensors. An FBG sensor can measure a distortion on a continuous basis with high accuracy and sensitivity, and the sensor section is compact owing to the use of optical fiber. Furthermore, it facilitates measurement of a pulse wave signal by a very simple method of fixing it at a pulsation point. Except for a few issues, the FBG sensors having such characteristics are expected to be used as wearable sensors successfully in future.

Currently, there are very few products that can continuously measure blood pressure without using a cuff. In addition, pulse rate and stress load can be detected with commercially available wearable sensors. However, at the same time, there is no wearable sensor using which both breathing rate and blood pressure can be calculated. This is because of the issues related to the time resolution and detection sensitivity of the measurement signal. In contrast, the FBG sensor can calculate these vital signs with high accuracy. It can be used as a precious blood pressure monitor. Moreover, considering that hospitalized patients need to be monitored on a continuous basis in respect of the vital signs, it would be a major breakthrough if the sensors can be installed in textile products for ease of handling and installation. The above discussions lead to the conclusion that it is possible to use an FBG sensor for monitoring of vital signs with high accuracy.

Acknowledgements

This work was supported by JSPS KAKNHI Grant Number JP16H01805 and the Wearable vital signs measurement system development project at Shinshu University. This research is (partially) supported by the Creation of a development platform for

implantable/wearable medical devices by a novel physiological data integration system of the Program on Open Innovation Platform with Enterprises, Research Institute and Academia (OPERA) from the Japan Science and Technology Agency (JST).

Conflict of interest

The authors declare no conflict of interest.

Author details

Shouhei Koyama[1*] and Hiroaki Ishizawa[2]

1 Faculty of Textile Science and Technology, Shinshu University, Japan

2 Institute for Fiber Engineering, Shinshu University, Japan

*Address all correspondence to: shouhei@shinshu-u.ac.jp

References

[1] Cabinet Office, Government of Japan. White Paper on Aging Society [Internet]. 2018. Available from: http://www8.cao.go.jp/kourei/whitepaper/w-2018/zenbun/pdf/1s1s_01.pdf [Accessed: November 15, 2018]

[2] Microsoft Co., Ltd. Glabella: Continuously Sensing Blood Pressure Behavior using an Unobtrusive Wearable Device [Internet]. 2017. Available from: https://www.microsoft.com/en-us/research/wp-content/uploads/2017/09/2017-imwut17-holz_wang-Glabella-Continuously_Sensing_Blood_Pressure_Behavior_using_an_Unobtrusive_Wearable.pdf [Accessed: November 15, 2018]

[3] Apple Inc. Apple Watch [Internet]. 2018. Available from: https://support.apple.com/en-am/HT204666 [Accessed: November 15, 2018]

[4] Seiko Epson Corp. Pulsense [Internet]. 2018. Available from: https://global.epson.com/innovation/core_technology/wearable/vital_sensing.html [Accessed: November 15, 2018]

[5] Wille J, Braams R, van Haren WH, van der Werken C. Pulse oximeter-induced digital injury: Frequency rate and possible causative factors. Critical Care Medicine. 2000;**28**(10):3555-3557

[6] Kellher JF, Ruff RH. The penumbra effect: Vasomotion-dependent pulse oximeter artifact due to probe malposition. Anesthesiology. 1989;**71**(5):787-791

[7] Tam HY, Liu SY, Guan BO, Chung WH, Chan TH, Cheng LK. Fiber Bragg grating sensors for structural and railway applications. In: Proceedings of International Society for Optical Engineering (SPIE). Photonics Asia; 8-12 November 2004; Beijing, China. 2004. pp. 85-97

[8] Wei CL, Lai CC, Liu SY, Chung WH, Ho TK, Tam HY, et al. A fiber Bragg grating sensor system for train axle counting. IEEE Sensors Journal. 2010;**10**(12):1905-1912. DOI: 10.1109/JSEN.2010.2049199

[9] Elsarnagawy TD, Haueisen J, Farrag MA, Ansari SG, Fouad H. Embedded fiber Bragg grating based strain sensor as smart costume for vital signal sensing. Sensor Letters. 2014;**12**(11):1669-1674. DOI: 10.1166/sl.2014.3382

[10] Spillman WB Jr, Mayer M, Bennett J, Gong J, Meissner KE, Davis B, et al. A 'smart' bed for non-intrusive monitoring of patient physiological factors. Measurement Science and Technology. 2004;**15**(8):1614-1620. DOI: 10.1088/0957-0233/15/8/032

[11] Hao J, Jayachandran M, Kng PL, Foo SF, AungAung PW, Cai Z. FBG-based smart bed system for healthcare applications. Frontiers of Optoelectronics. 2010;**3**(1):78-83. DOI: 10.1007/s12200-009-0066-0

[12] Sakaguchi A, Kato M, Ishizawa H, Kimura H, Koyama S. Fabrication of optical fiber embedded knitted fabrics for smart textiles. Journal of Textile Engineering. 2016;**62**(6):129-134. DOI: 10.4188/jte.62.129

[13] Koyama S, Ishizawa H, Sakaguchi A, Hosoya S, Kawamura T. Influence on calculated blood pressure of measurement posture for the development of wearable vital sign sensors. Journal of Sensors. 2017;**2017**:8916596. DOI: 10.1155/2017/8916596

[14] Yoshino T, Sano Y, Ota D, Fujita K, Ikui T. Fiber-Bragg-grating based single axial mode Fabry-Perot interferometer and its strain and acceleration sensing applications. Journal of Lightwave

Technology. 2016;**34**(9):2240-2250. DOI: 10.1109/JLT.2016.2521440

[15] Todd MD, Johnson GA, Chang CC. Passive, light intensity-independent interferometric method for fiber Bragg grating interrogation. Electronics Letters. 1999;**35**(22):1970-1971. DOI: 10.1049/el:19991328

[16] Kadowaki H, Hayase T, Funamoto K, Sone S, Shimazaki T, Jibiki T, et al. Blood flow analysis in carotid artery bifurcation by two-dimensional ultrasonic-measurement-integrated simulation. Journal of Biomechanical Science and Engineering. 2014;**10**(1): 14-00266. DOI: 10.1299/jbse.14-00266

[17] Koyama S, Ishizawa H, Hosoya S, Kawamura T, Chino S. Stress loading detection method using the FBG sensor for smart textile. Journal of Fiber Science and Technology. 2017;**73**(11):276-283. DOI: 10.2115/fiberst.2017-0042

[18] Takazawa K, Fujita M, Kiyoshi Y, Sakai T, Kobayashi T, Maeda K, et al. Clinical usefulness of the second derivative of a plethysmogram (acceleration plethysmogram). Cardiology. 1993;**23**:207-217

[19] Koyama S, Ishizawa H, Fujimoto K, Chino S, Kobayashi Y. Influence of individual differences on the calculation method for FBG-type blood pressure sensors. Sensors. 2017;**17**:1-48. DOI: 10.3390/s17010048